Journal of MATERIALS RESEARCH

Invited Paper
DOI:10.1557/s43578-021-00184-8

MULTISCALE MATERIALS MODELING OF INTERFACE-MEDIATED THERMOMECHANICAL BEHAVIOR

FOCUS ISSUE

Lattice dislocation induced misfit dislocation evolution in semi-coherent {111} bimetal interfaces

Alex Selimov[1,a], Shuozhi Xu[2], Youping Chen[3], David McDowell[1,4]

[1] Department of Materials Science and Engineering, Georgia Institute of Technology, Atlanta, GA 30332, USA
[2] Department of Mechanical Engineering, University of California, Santa Barbara, CA 93106, USA
[3] Department of Mechanical and Aerospace Engineering, University of Florida, Gainesville, FL 32611, USA
[4] Woodruff School of Mechanical Engineering, Georgia Institute of Technology, Atlanta, GA 30332, USA
[a] Address all correspondence to this author. e-mail: aselimov3@gatech.edu

Received: 7 January 2021; accepted: 20 March 2021

David McDowell was an editor of this journal during the review and decision stage. For the JMR policy on review and publication of manuscripts authored by editors, please refer to http://www.mrs.org/editor-manuscripts/.

The study of dislocation plasticity mediated by semi-coherent interfaces can aid in the design of certain heterostructured materials, such as nanolaminates. The evolution of interface misfit patterns under complex stress fields arising from dislocation pileups can influence local dislocation/interface interactions, including effects of multiple incoming dislocations. This work utilizes the Concurrent Atomistic-Continuum modeling framework to probe the evolution of misfit structures at semi-coherent Ni/Cu and Cu/Ag interfaces impinged by dislocation pileups generated via nanoindentation. A continuum microrotation metric is computed at various stages of the indentation process and used to visualize the evolution of the interface misfit dislocation pattern. The stress state from approaching dislocations induces mixed contraction and expansion of misfit dislocation structures at the interface. A lower number of misfit nodes per unit interface area coincides with greater localized deformation with regard to atoms near misfit nodes for Ni/Cu. The decreased misfit node spacing for Cu/Ag alternatively distributes the restructuring associated with plastic deformation over a larger percentage of atoms at the interface. Interface sliding facilitated by misfit dislocation motion is found to facilitate deformation extending into the bulk lattices centered on misfit nodes. The depth of penetration of those fields is found to be greater for Ni/Cu than for Cu/Ag.

Introduction

Heterostructured materials are characterized by heterogeneous domains with significantly different material properties that interact cooperatively to improve overall mechanical behavior. These heterogeneous domains consist of multi-modal or graded distributions of grain size [1, 2], texture [3], or phase [4–6]. One particular heterostructured material which has garnered much interest is the nanolaminate, which consists of alternating phases in a lamellar structure with layer thicknesses in the range of several to tens of nm. They exhibit improved properties compared to their bulk constituents [7–9] due to the mediating influence of interphase boundaries on dislocation absorption, desorption, or direct transmission. These interfaces mediate the transmission of plastic deformation between layers, depending on the interface structure [10, 11]. The influence of complex stress states, such as those induced by approaching dislocations, can impact interface misfit patterns [12]. Changes to interface misfit dislocation spacing, resulting from applied shear stress [13, 14], has been shown to change various aspects of interface structure and energy minimization processes [15]. This can contribute to the interface blocking strength through increased misalignment of slip planes [16] or by increased misfit dislocation density at the lattice dislocation impingement [17]. Computational methods are necessary to explore such complexities of interface evolution during plastic deformation, since in situ transmission electron microscopy is difficult to perform [18].

The evolution of semi-coherent interface structures during dislocation transmission and/or restructuring under loading has previously been investigated using atomistic methods. Shao et al. [19] studied the energy minimized spiral patterns of misfit dislocations entering misfit dislocation junctions, referred to as "nodes," in the Ni/Cu system and found that the expansion and contraction of the nodal structures under mechanical shearing affected their ability to absorb and emit point defects. Asymmetrical non-Schmid nucleation of dislocations from misfit node structures in Ni/Cu semi-coherent interfaces under various in plane boundary conditions was found by Chen et al. [14], revealing the inherent heterogeneity of these interfaces and the need for atomic resolution to capture evolution of interface plasticity. Interface sliding, facilitated by migration of misfit dislocations along the interface plane, was explored for the Ni/Cu system by Chen et al. [14] and for the Ni/Ni_3Al system by Yang et al. [20] through molecular dynamics (MD) simulations. These studies lead to the conclusion that the misfit nodes initiate plastic deformation under loading, either by acting as a dislocation source or facilitating interface sliding under applied shear stress. Changes to interface energy minimization pathways for different misfit node spacings has been studied for Ni/Cu and Cu/Ag systems by Shao et al. [21], who found that the degree of spiraling at misfit nodes is controlled by the misfit node spacing. This implies that misfit dislocation pattern evolution under loading may occur along different pathways for different misfit node spacings. However, these atomistic studies on semi-coherent interfaces are generally limited to either a single misfit node or a small number of misfit nodes for relatively small computation cells with periodic boundary conditions applied within the interface plane and homogeneous stress/deformation states applied to the cell boundary. This accordingly limits or constrains the range of misfit pattern evolution observed. Discussion of models with larger interfaces that contain more misfit nodes is lacking in the literature, likely due to the characteristic length-scale of the misfit pattern associated with some common interfaces, such as the interface between Ni/Cu [20], and complex energy landscapes which require many iterations for convergence. Both factors make atomistic studies difficult due to computational costs. However, such studies are essential when considering highly heterogeneous interface stress fields associated with dislocation pileup impingement; this phenomenon is generally beyond the capability of small periodic cell sizes used in full MD simulations.

To facilitate studies of larger interface sections and the evolution of their misfit patterns in the presence of shear gradients, we consider a fully concurrent approach to coarse-graining of atomistics. In this regard, we mention the coarse-graining Quasi-Continuum (QC) method and variants [22, 23] and the domain decomposition-based Coupled Atomistic Discrete Dislocation method [24, 25]. The interested reader can consult prior reviews of these schemes for concurrent multiscale modeling of dislocation reactions [26–28]. We employ instead the Concurrent Atomistic-Continuum (CAC) [29] method in the present study, as it can address the migration and exchange of arrays of dislocations in coarse-grained and fully resolved atomistic regions without adaptive mesh refinement, does not require any constitutive relation beyond the interatomic potential, and avoids domain decomposition based on different constitutive models and associated transfer of information across domains. Accordingly, it efficiently captures long range fields in the lattice using usual nonlocal atomistics, while allowing fully resolved dislocation–defect reactions. Coarse-graining is achieved in bulk regions to reduce degrees of freedom, while full atomistic resolution is maintained within regions that undergo large extent of atomic restructuring to ensure the accuracy of the reaction pathway. Dislocations are accommodated naturally along interelement discontinuities, fully capturing long range elastic fields [30] and reducing the required degrees of freedom for modeling dislocation arrays. Dislocations seamlessly pass between coarse-grained regions and atomistic regions along the discontinuities in the finite element mesh without requiring heuristics to transfer dislocation information between regions. CAC has been applied to a variety of problems which require extended domains to model inhomogeneous structure evolution. Dislocation pileups and their interactions with a variety of obstacles have been studied including void and inclusion bypass [31]. Models of approximately 86 million equivalent atoms (42,000 finite elements) have been used to study the nucleation, growth, and interaction of dislocation loops in Cu, Al, and Si [32]. Of particular relevance to the current research are studies on the transmission of dislocations across coherent twin boundaries in Cu and Al [33], coherent twin boundaries and symmetric tilt grain boundaries in Ni [34], and Si/Ge semi-coherent interfaces [35], as well as on semi-coherent interface structures in PbTe/PbSe bilayers with semi-coherent interfaces [36]. All these studies utilized the mesh discontinuity to accommodate dislocations, reducing required degrees of freedom far from the interface, while maintaining the interfaces at full atomistic resolution. As such, it was possible to observe the interaction of dislocation arrays with interfaces and the evolution of the interface structure with simulation domains approaching the micron scale. The largest CAC model to date employed over 10 billion atoms [37]. These types of problems are intractable for atomistic methods due to the required domain sizes. Other types of concurrent multiscale methods such as the QC method may struggle as the interactions between these defect arrays and extended interface dislocations may require adaptive remeshing to full atomistic resolution over much of the domain.

In this work, periodic energy minimization is utilized in a so-called quasistatic CAC approach [30] to assess the near-equilibrium lattice dislocation induced misfit pattern evolution that is typical of thermally-assisted deformation. This avoids the high effective strain rates associated with MD which can result in a physical overdriven reactions [38]. Entropic effects are not considered in this work. To study thermally activated processes, quasistatic simulations should minimally be augmented with harmonic transition state theory [39, 40] or use of the Meyer–Neldel compensation law to estimate activation entropy [41, 42] based on activation enthalpy of dislocation-interface reactions computed, for example, using nudged elastic band (NEB) methods [43]. Studying the mechanically induced misfit pattern evolution under quasi-static conditions prior to interactions with lattice dislocations can more realistically inform reduced order models, as the local misfit dislocation environment is known to affect slip transmission [17, 35] and is not too far from equilibrium. Capturing this evolution necessitates the use of large interface segments to allow for non-uniform misfit structure evolution. Important implications regarding the interface misfit structure stability and interface shear strength can furthermore aid in the design of interfaces used for hierarchically structured nanolaminates.

Non-uniform interface sliding under complex stress fields ahead of dislocation pileups

The first stage in the interface misfit dislocation pattern evolution with the approach of the lead dislocation in each pileup is the motion of misfit dislocations and their junctions, referred to as "nodes." It is known that under shear loading conditions, semi-coherent interfaces can exhibit interface sliding via the motion of misfit dislocations along the interface plane [14, 20, 35]. Interface sliding generally originates in the misfit nodes as they readily glide under shear conditions in bimetal semi-coherent interfaces, such as Ni/Cu and Cu/Ag. A shear stress induced by indentation generated dislocations drives the evolution of misfit patterns for the investigated geometries, as seen for Ni/Cu in Fig. 1 where the projected impingement of the dislocation pileup slip planes are denoted by dotted lines. These lines separate the regions of the interface which are on the compressive side of the incoming dislocations and the portions of the interface which are on the tensile side. This results in sharp σ_{zx} shear stress gradients at the impingement lines that cause the non-uniform expansion/contraction of the misfit patterns. This is more pronounced in the Ni/Cu interface than in the Cu/

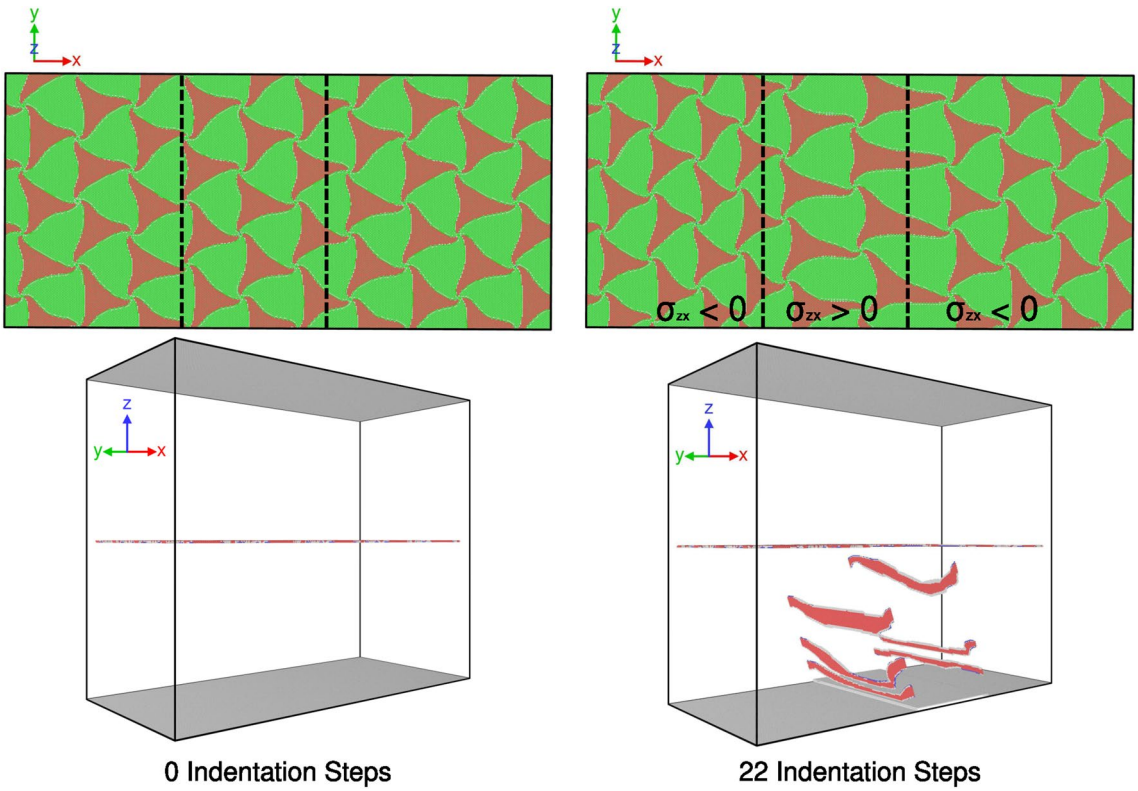

Figure 1: Common neighbor analysis for all atoms at interface (top) and with FCC atoms hidden (bottom) at two different indentation steps for Ni/Cu. Red atoms are in an HCP structure, blue atoms are in a BCC structure and gray atoms are in undefined structures. Deformation of misfit structures occurs as heterogeneous compression/extension of the nodal spacing in the *x* direction. Dashed lines in the top figures represent the impingement line of the incoming dislocations on the interface.

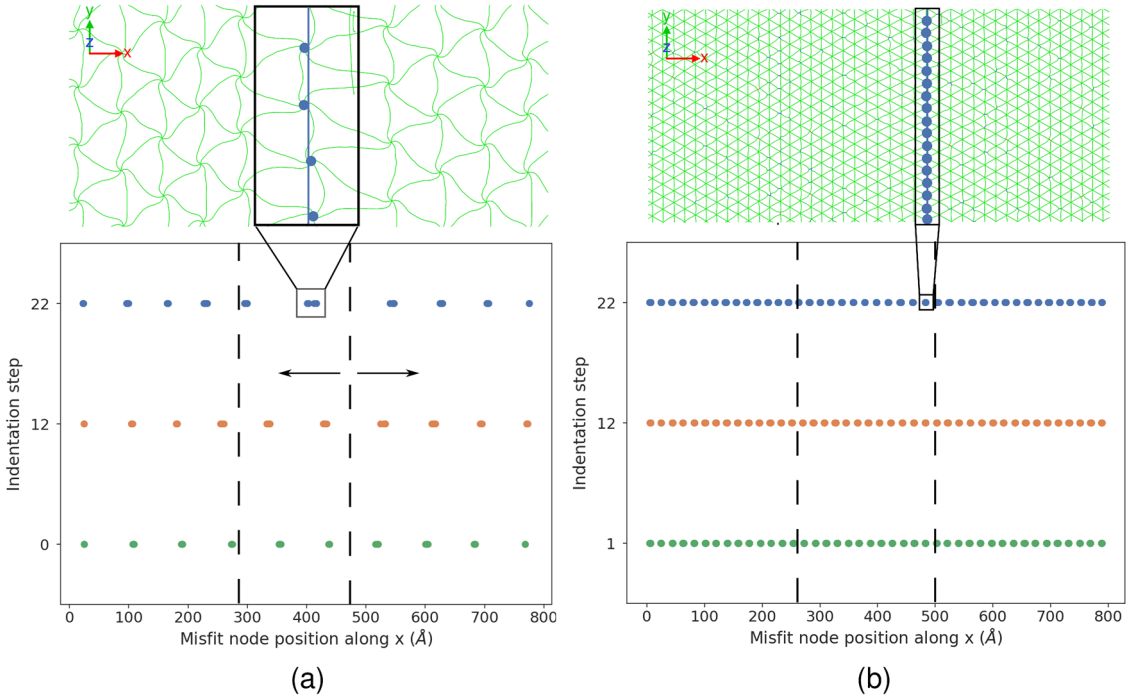

Figure 2: Position of dislocation nodes along x direction for three different time steps for (a) Ni/Cu and (b) Cu/Ag. Dashed lines represent the slip plane impingement lines. Multiple nodes at the interface have very close *x*-positions due to the misfit periodicity in the current orientation as shown in the exploded view. The arrows indicate the direction of misfit node motion away from the impingement line. Colors denote different indentation steps.

Ag interface. The evolution of the misfit node position in the *x* direction helps to illustrate this behavior and is presented in Fig. 2. The dislocation nodes in the Ni/Cu interface are repulsed primarily from the rightmost pileup impingement line in the interface because dislocations progress first along the right edge of the indenter, as seen in Fig. 1. By comparison, only relatively small shifts in misfit node position are observed for the Cu/Ag interface.

This differences in the evolution of misfit patterns can be attributed primarily to the misfit dislocation spacing. Smaller regions of coherency at the Cu/Ag interface reduces the distance that dislocations can freely glide, while the increased density of misfit nodes serves to block the motion of other misfit dislocations or nodes. For motion to occur it must occur cooperatively over larger portions of the interface. Decreasing misfit node spacing for the Ni/Cu interface, for example by twisting one of the crystals relative to the other [21], is expected to lead to increased misfit structure stability. It is also important to note that the motion of misfit nodes is away from the incoming lattice dislocation. It is expected that misfit nodes would be strong obstacles to slip transmission due to their low shear strength which could promote dislocation core spreading within the interface plane. Decreased misfit spacings have been found to result in increased resistance to slip transfer [35]. Because the Cu/Ag interface is more stable, this motion of misfit nodes does not occur over significant distances and interactions of incoming lattice dislocations with misfit nodes are more likely, possibly contributing to further increases in blocking strength. In the case of sessile misfit nodes, such as in metal/ceramic semi-coherent interfaces [43], dislocations will bow out in opposite directions, depending on the sign of the induced shear stress, with dislocation segments pinned by the misfit nodes. The degree to which the dislocations bow out will increase as additional dislocations are generated in the pileup. This type of spatially varying interface structure evolution is generally missed in atomistic methods due to low number of misfit nodes modeled resulting from limitations in the size of interface sections which can be modeled.

Effects of misfit node spacing on the evolution of misfit dislocation patterns

The microrotation is used to quantitatively characterize the nature of the interface deformation as components of the microrotation vector can capture different aspects of the deformation, as shown in Fig. 3 for Ni/Cu and in Fig. 4 for Cu/Ag. Because the misfit dislocations are constrained to the *x*–*y* interface plane, the first component of the microrotation captures the local rotations associated with motion of dislocations in the *y* (or [011]) direction and the second component captures the motion of dislocations in the *x* (or $[\bar{2}1\bar{1}]$) direction; these microrotation components register relative rotation of atoms across the interface

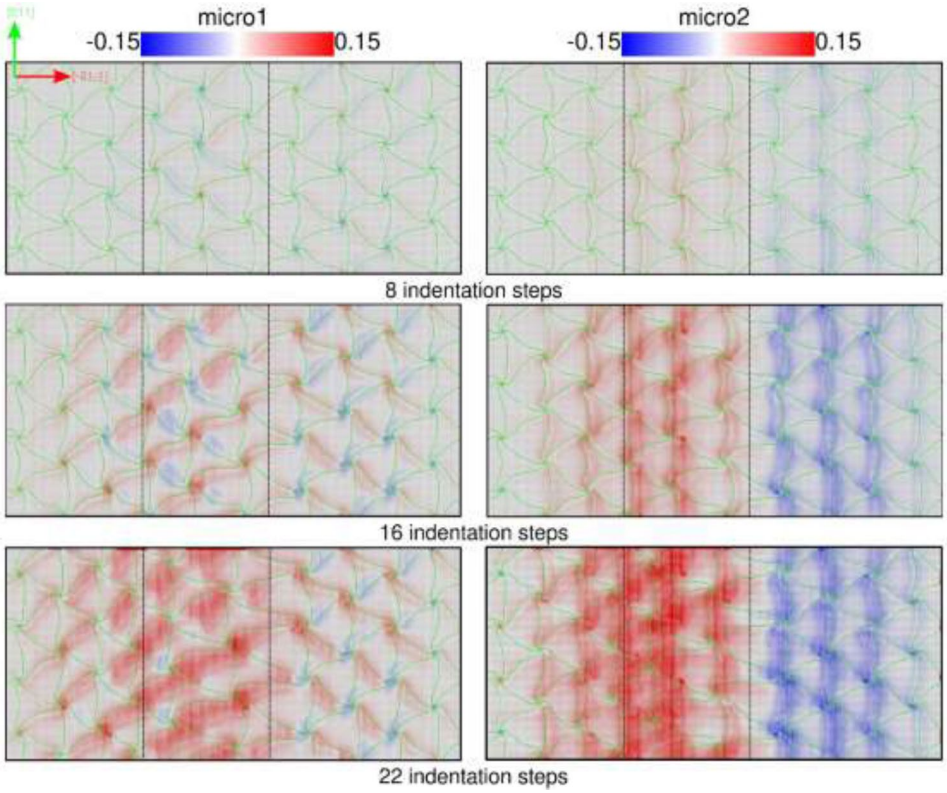

Figure 3: The first (micro1) and second (micro2) components of the microrotation vectors at various indentation steps for the Ni atoms at the Ni/Cu interface. It is seen that at earlier indentation steps the microrotation is maximized at the misfit nodes and then increases along the dislocation lines as indentation progresses.

plane. The third component of the microrotation captures both and is not presented due to its lack of specificity in this regard.

At earlier indentation steps, as seen for Ni/Cu in Fig. 3, the microrotation fields are primarily concentrated at the misfit nodes with some degree of spreading along misfit dislocation lines. As stress increases due to the indentation, the microrotation fields begin to increase in magnitude in the coherent and stacking fault portions of the interface. This indicates that the interface deformation begins at the misfit nodes, proceeds along the misfit dislocation lines, and through misfit dislocation glide to the rest of the interface. Local differences in the sense of the microrotation, seen as alternating blue and red fields, relates to the non-uniform local rotation of the lattice structure required for unidirectional misfit node motion in Ni/Cu [14]. Misfit nodes which display these alternating microrotation fields experience little net movement in the [011] direction, suggesting that the σ_{zy} component of the shear stress is small. At these earlier stages, the development of the first microrotation component can be attributed primarily to restructuring required for motion of the misfit nodes in the $[\bar{2}1\bar{1}]$ direction. This non-uniform misfit dislocation glide which is seen to accompany the misfit node motion does however result in a change to the spacing of the dislocation lines at their points of intersection with the incoming lattice dislocation slip planes. Coherent FCC regions near the impingement lines grow in size while the stacking fault regions shrink, causing both expansion/contraction to the dislocation intersection point spacing along the impingement line. Maximum observed changes approached 9 Å. The literature shows that the misfit dislocation spacing affects slip transmission [35]. This type of evolution of misfit structures ahead of incoming lattice dislocations may therefore be non-negligible when considering slip transmission. The second component of the microrotation shows a shift in the direction of lattice rotation which accompanies misfit node motion when crossing the rightmost dislocation impingement line. This shift in the sense of the microrotation is associated with the opposite signs of σ_{zx} on either side of the line which drives the motion of misfit nodes in opposite directions.

The microrotation fields at the Cu/Ag interface presented in Fig. 4 have similar overall patterns to those of Ni/Cu, indicating that the global motion of misfit nodes occurs along the same directions. Lower magnitudes for both components of the microrotation are seen as lower intensities for Cu/Ag and suggest a lower misfit node mobility within the interface. The regions with

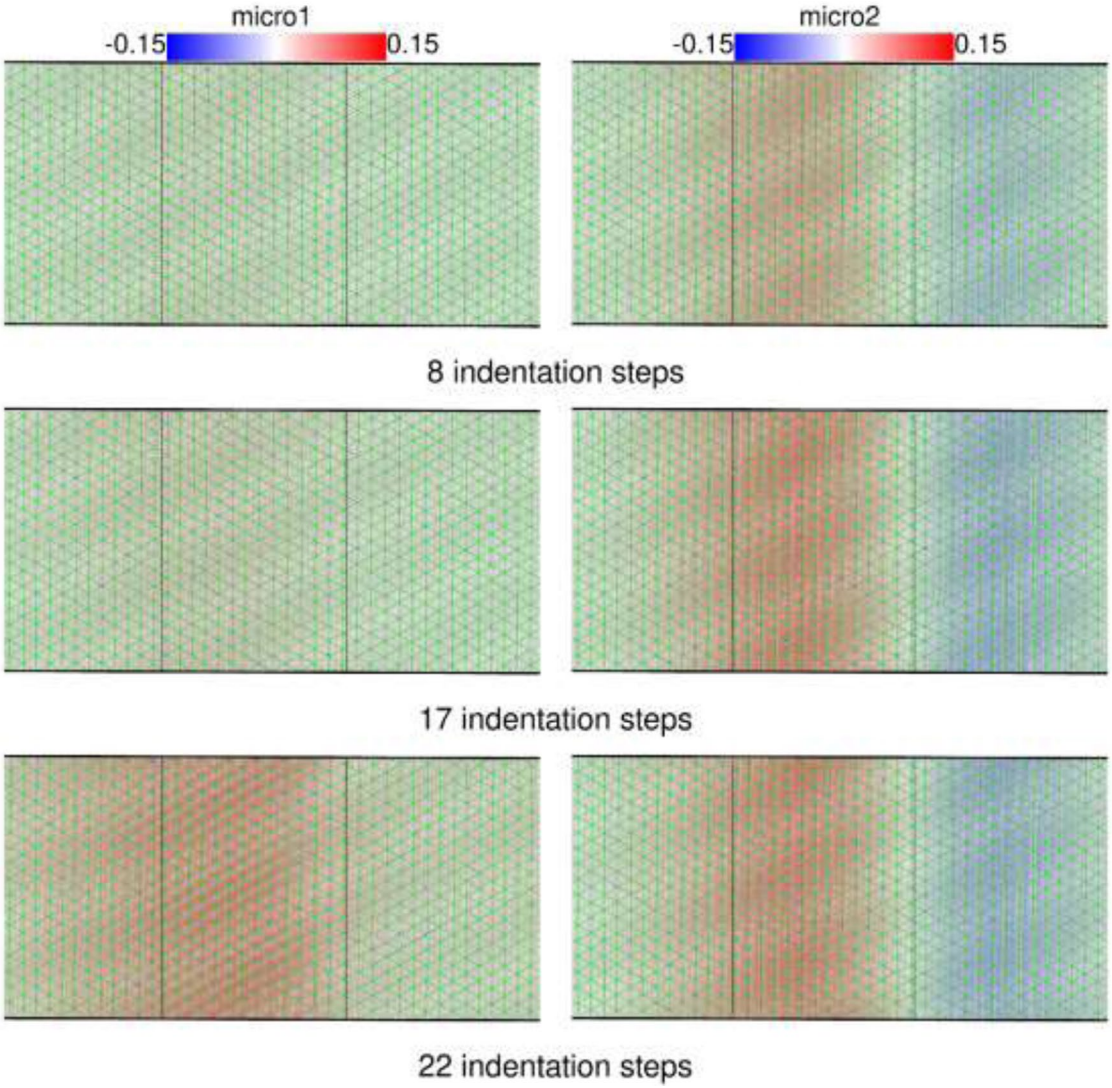

Figure 4: The first (micro1) and second (micro2) components of the microrotation vectors at various indentation steps for the Cu atoms at the Cu/Ag interface. Smoother fields of microrotation are evident when compared to those found in the Ni/Cu interface, shown in Fig. 3.

alternating sense for the first component of the microrotation, observed for Ni/Cu, are missing for Cu/Ag. This implies that the net motion of misfit nodes in the $[\bar{2}1\bar{1}]$ direction does not require local rotation of the atomic structure about the [011] direction. The spiraling of misfit dislocations as they enter the misfit nodes, seen in Ni/Cu but not observed for Cu/Ag, may be the cause for this difference. Maintaining the spiral pattern at the misfit nodes may require larger deviations from the equilibrium lattice structure when compared to the motion of straight dislocation segments in Cu/Ag. Smoother fields are also observed, which indicates the increased participation of atoms at the interface in the deformation for Cu/Ag due to the increased percentage of atoms in the vicinity of misfit dislocations and misfit nodes (the number density of nodes in the interface plane is higher). The higher magnitudes and comparatively lack of smooth fields for the microrotation observed in Ni/Cu arise from the lower percentage of atoms in the vicinity of misfit dislocations and misfit nodes.

The misfit node spacing therefore affects the interface deformation in two primary ways. First, the misfit node spacing controls the stability of the interface structure. A decreased misfit node spacing results in a more uniform distribution of deformation across interface atoms. The misfit dislocations and misfit nodes under the same shear stress condition glide in the same direction. This is observed by the smooth microrotation fields and the uniform sense of the microrotation for atoms on the same sides of the incoming dislocation impingement lines. Alternatively, the larger

misfit dislocation spacings of Cu/Ni exhibit significant deformation of the misfit dislocation structure, including changes to misfit dislocation spacing along the impingement lines resulting from misfit dislocation glide in variant directions. These changes to the misfit structure of Ni/Cu may cause decreases to the slip transmission resistance of the interface. Second, in addition to significant distortions of the misfit patterns, localization of deformation is observed. This arises due to the decreased number of atoms in the vicinity of misfit dislocations which participate in the misfit pattern evolution. This is observed by the strongly concentrated microrotation fields which are concentrated at the misfit dislocations and misfit nodes.

Quantitative analysis of interface deformation through microrotation distributions

To better quantify these differences in misfit pattern evolution, the fraction of atoms containing different microrotation component values is presented in Fig. 5. This is done by binning the microrotation component magnitudes for atoms within 2 nm of the interface and then normalizing the number of atoms with a specific microrotation component magnitude by the total number of atoms in all bins. For all plots, at lower indentation steps the microrotation values are narrowly distributed around zero. As the dislocation approaches the interface, the distribution of

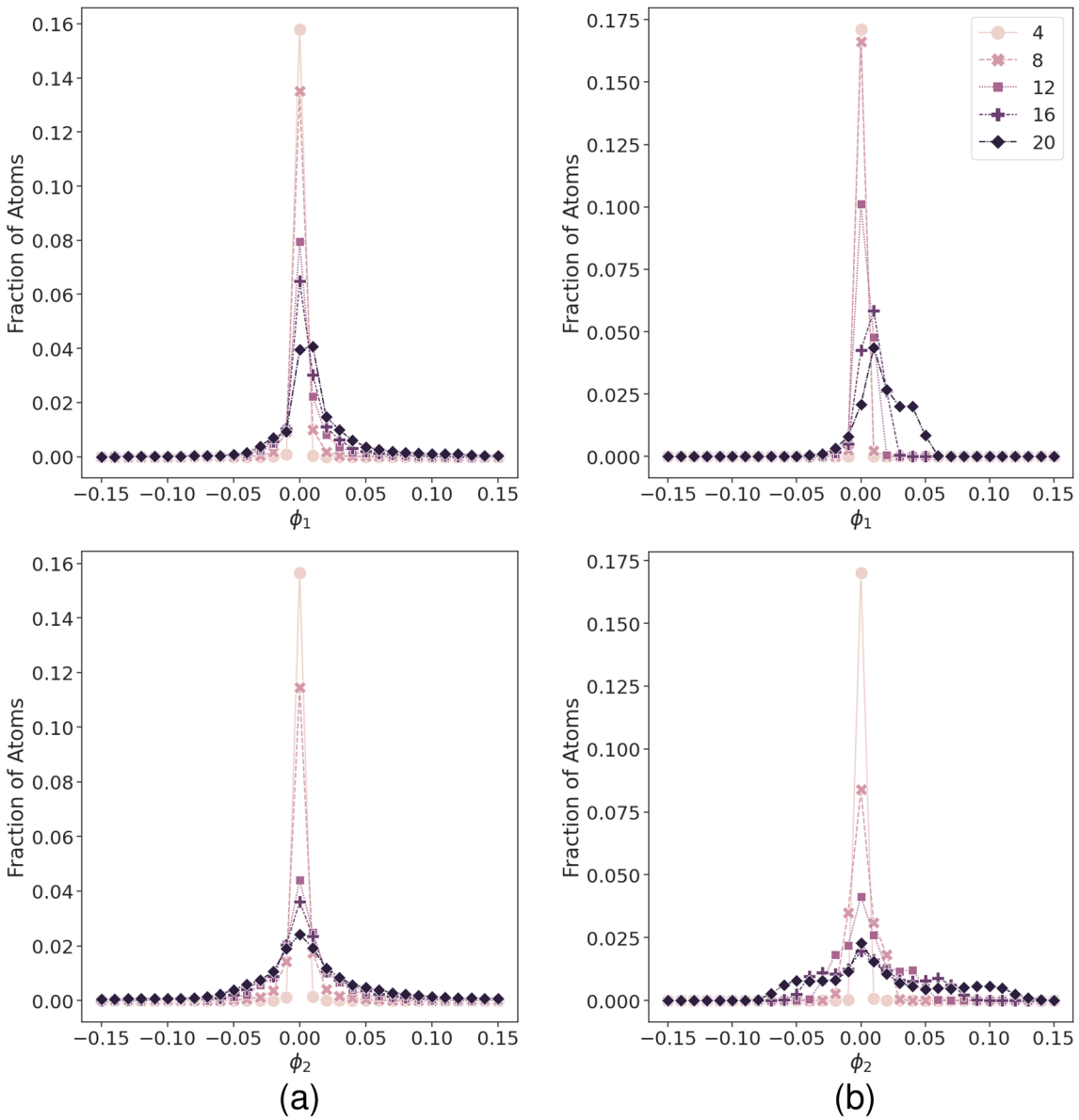

Figure 5: Binned microrotation versus frequency for (a) Ni/Cu and (b) Cu/Ag. For both systems, φ_2 is distributed symmetrically around 0 with a slight skew to positive values. φ_1 shows a clear skew to positive values and is more equally distributed at higher values for Cu/Ag.

φ_2 begins to broaden symmetrically with an associated drop in the number of atoms reporting zero microrotation. The tails of the distribution for Cu/Ag tend to hold higher fractions of atoms than the tails of the distribution for Ni/Cu which drop to zero more rapidly. This quantitatively shows that decreased misfit node spacing results in a more uniform distribution of deformation across the interface. φ_1 shows a similar broadening of the distribution and a drop in the number of atoms experiencing zero microrotation but with a skew to positive values at larger timesteps. The increased symmetry observed for the distribution of this component for Ni/Cu relates to the more complex rotation of the atomic structure around misfit nodes required for accommodating the motion of the spiral patterned misfit dislocations.

Figure 5 may give the impression that the Cu/Ag interface experiences greater deformation of misfit patterns when compared to Ni/Cu due to the higher number of atoms that experience larger microrotation fields. However, calculating the maximum value for the microrotation of atoms at the interface for both systems shows higher maximum microrotation values for Ni/Cu at every timestep, as seen in Fig. 6. These maximum values are also multiple factors larger than the average microrotations calculated for the Ni/Cu interface, as seen from Fig. 5. This is indicative of large deviations in deformation experienced by interface atoms and the localization of plasticity to small regions of atoms around misfit nodes. In the case of Cu/Ag, the maximum values are much closer to the average microrotation for atoms at the interface, which indicates a more uniform distribution of deformation. Magnitudes for microrotation of approximately 0.15 indicate full slip and magnitudes of 0.09 indicate partial slip associated with atoms located in a stacking fault separating partial dislocations [44]. The maximum values of microrotation for Cu/Ag indicate that at most a local atomic neighborhood at the interface has undergone full slip whereas the maximum values for Ni/Cu, well above 0.15, suggest larger and more complex degree of restructuring.

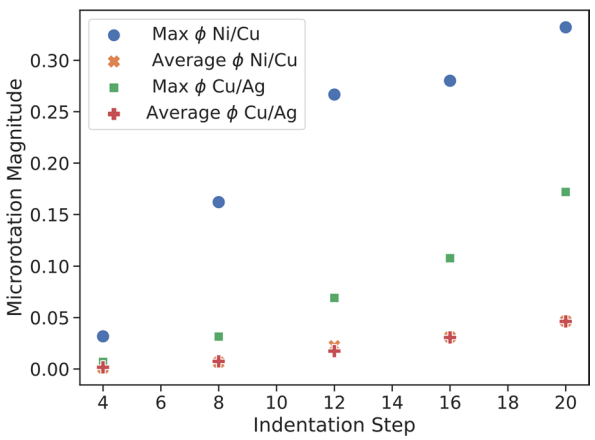

Figure 6: Maximum and average microrotation magnitudes for atoms near the interface. Larger maximum magnitudes are measured for Ni/Cu, but average values are similar for both interfaces; this suggests similar total amounts of interface deformation occurs, but with increased localization for Ni/Cu.

In summary, through the numerical analysis of the microrotation fields it is evident that localization of plasticity occurs to a larger degree for the Ni/Cu interface. The distributions of microrotation magnitudes among interface atoms confirm this as seen by a narrower distribution of microrotations for Ni/Cu than for Cu/Ag. The larger ratio of maximum microrotation magnitude to average microrotation magnitude provides additional validation of this conclusion.

Deformation fields extend from misfit nodes and can be characterized through the microrotation

Associated with misfit dislocation motion is a deformation field that extends into the bulk lattice. This is also evident from the microrotation, where "islands" containing regions of atoms which have undergone deformation extend from the misfit nodes at the interface; this is shown in Fig. 7a for Ni/Cu and Fig. 7b for Cu/Ag. These islands grow in size and magnitude as the indentation progresses, extending further into both bulk lattices. The extended deformation fields originating at the misfit nodes agree with previous findings that misfit nodes serve as dislocation nucleation sites for the Ni/Cu semi-coherent interface [13, 14]. Extended microrotation fields from grain-boundaries have previously been associated with dislocation nucleation from those boundaries [44]. These microrotation fields penetrate deeper into the bulk lattices for the Ni/Cu interface than for the Cu/Ag interface, which is indicative of extended deformation of the crystal lattice as a result of the change of configuration of the misfit dislocations. To quantify the extent that these fields grow into the bulk layer, the atoms are binned along the z direction in bins of approximately 2 Å thickness. The average microrotation magnitude for atoms within the bin is then calculated and compared for Ni/Cu and Cu/Ag in Fig. 7.

Magnitudes of both microrotation components tend to approach similar values far from the interface. The Ni/Cu microrotation fields decay over larger distances than the measured Cu/Ag fields, indicating that the significant motion of misfit dislocations must be accommodated by deformation of the atomic structure in neighboring planes. Similar extended deformation fields associated with the interface restructuring that occurs upon minimization of the unrelaxed interface structure, as seen in [19], are likely the primary source of error measured in the mesh sensitivity study presented in the Methodology section and Fig. 9. This error arises from the constraint imparted by the

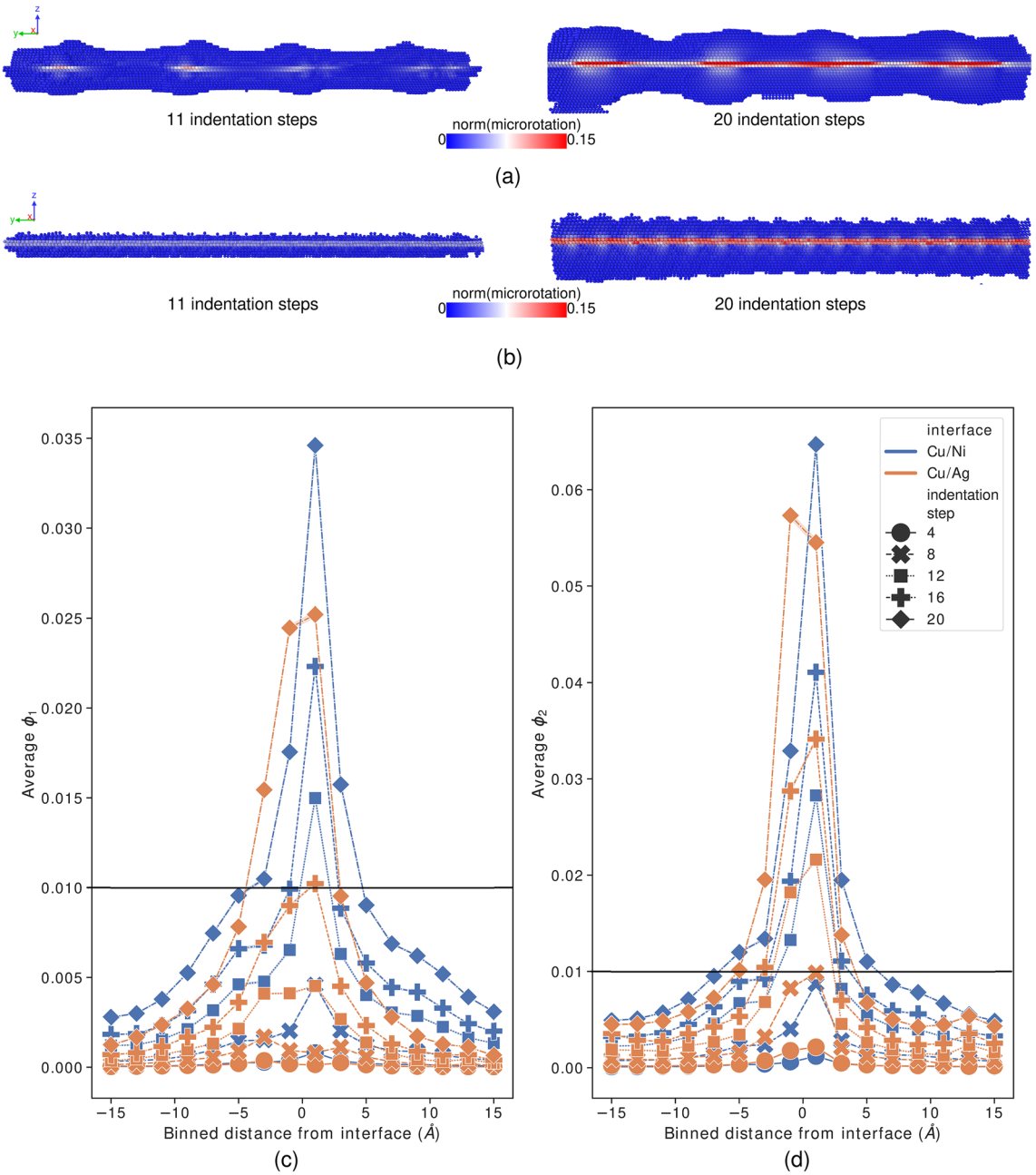

Figure 7: Cross section of interface with atoms colored by magnitude of the microrotation vector for (a) Ni/Cu and (b) Cu/Ag interfaces. Atoms with microrotation magnitudes less than 0.01 are hidden. The islands are much larger for Ni/Cu, implying deformation of lattice structure farther from interface, and in both cases extend primarily from misfit nodes. (c) Cu/Ag and (d) Ni/Cu average microrotation magnitudes for different components versus distance shows larger microrotation fields away from interface for Ni/Cu. The horizontal black lines at 0.01 microrotation emphasize regions of non-negligible microrotation.

coarse-graining scheme which is not able to fully capture the non-linear deformation fields. In the studied geometries, the atomistic region was large enough to fully capture this extended lattice restructuring. The reader can refer to the Methodology section for a more in-depth discussion of error introduced by the distance of the interface to the coarse-grained region.

The depth of penetration of the deformation fields originating from misfit nodes may be a measure of the interface's ability to nucleate dislocations and transmit slip, both processes requiring extended restructuring of the atomic structure. Because dislocation nucleation requires participation of neighboring planes, interfaces which have larger deformation

fields extending from misfit nodes likely have lower required critical stresses for dislocation nucleation. This analysis suggests that the smaller misfit node spacing in Cu/Ag corresponds to an increased stress required for dislocation nucleation from the interface. The effects of the observed complex deformation of the Ni/Cu interface misfit patterns on this critical stress for nucleation requires further study.

Conclusions

The evolution of interface structures in both Cu/Ag and Ni/Cu bilayers is studied in this article using the CAC methodology. The microrotation is calculated for every atom at the interface to quantify restructuring associated with the deformation of the interface misfit patterns. The primary findings of these studies are as follows:

- Dislocation stress fields can cause increasing degrees of deformation to interface misfit structures in which non-uniform expansion/contraction occurs.
- Misfit nodes are seen to glide away from slip plane impingement sites in Ni/Cu. This is expected to cause further decreases in the interface blocking strength as compared to Cu/Ag, in which lattice dislocations are more likely to impinge upon misfit nodes.
- Deformation of the misfit patterns at the Cu/Ag interface occurs more uniformly along the interface due to the higher misfit density. For Ni/Cu the deformation is localized at the fewer nodes that are present resulting in higher maximum magnitudes of deformation. This is quantitatively observed using the microrotation as a metric.
- Misfit pattern evolution is accompanied by regions of restructuring in the phase interiors which extend from the misfit dislocation nodes. The depth of penetration for these regions is larger in Ni/Cu due to the larger degrees of restructuring localized to the misfit dislocation nodes.

Future work will address various open questions. The extent to which the change in misfit pattern affects the interface blocking strength will be quantified. The degree to which the misfit node spacing impacts the slip transmission will be characterized through comparisons between Ni/Cu and Cu/Ag. The evolution of interface structure during sequential slip transmissions and associated changes in interface blocking strength will also be studied. The difference in Burgers vectors for both components in a bilayered material must be accommodated within the interface for slip transmission to occur which manifests as a step left on the interface. It is expected that the growth of this step will increase the interface blocking strength [45]. Increases to the blocking strength may result in a change in mechanism from slip transmission to a more favorable nucleation of dislocations from the step [46]. The increased stability of the Cu/Ag interface misfit structure and the lower misfit dislocation spacing, observed in this work, are expected to result in a higher blocking strength than that of Ni/Cu.

Methodology

Figure 8 presents a schematic of the model under investigation. These bicrystal models are partitioned into two coarse-grained regions for the bulk crystals and one atomistic region which contains the semi-coherent interface. The coarse-grained regions reduce the number of degrees of freedom while allowing for the transmission of dislocations from the surface of the model to the interface. This is very important in reducing computational time for periodic energy minimization. To ensure that the dislocations are represented correctly in the coarse-grained domain, 3D rhombohedral elements are used that utilize a second nearest neighbor interpolation scheme and have all faces aligned to {111} slip planes [30]. Each element in the coarse-grained domain represents 15,625 atoms. Bicrystal models comprised of alternating Cu and Ni layers or Cu and Ag layers are studied, each containing one semi-coherent $(11\bar{1})$ interface. These models are generated by stacking two regions of either Cu and Ni or Cu and Ag in the z direction and then performing energy minimization using the fast inertial relaxation engine (FIRE) [47]. Calculated misfit node spacings are 9.5 nm for the Ni/Cu interface and 2.2 nm for the Cu/Ag which agree well with computational studies found in the literature [21]. Additionally, dislocations entering misfit nodes are seen to form a spiral pattern characteristic of Ni/Cu [19] but not observed for undeformed Cu/Ag interfaces [21]. The misfit dislocation densities for the relaxed interfaces are 0.39028 and 1.5673 nm^{-1} for Ni/Cu and Cu/Ag respectively.

To determine the minimum number of atomic layers between the interface and coarse-grained regions needed to fully capture relevant interface reconstructive reactions, a mesh sensitivity study is conducted on the Ni/Cu semi-coherent interface. The trilinear shape function used in the finite elements within the coarse-grained domains does not accurately capture these non-linear displacement fields, inhibiting the correct development of the interface misfit structure. Therefore, it is critically important to quantify the minimum distance from interface to coarse-grained region to ensure correct modeling of interface evolution. Models containing an unrelaxed semi-coherent Ni/Cu interface with different numbers of atomic layers at the interface were energy minimized. We built a reference model with 20 atomic layers extending from the interface as further increases in the number of atomic layers yielded fewer benefits to accuracy. A fully atomistic reference model was not used due to the simulation cell sizes, which would require approximately 40 million atoms. Each test model was compared to the reference

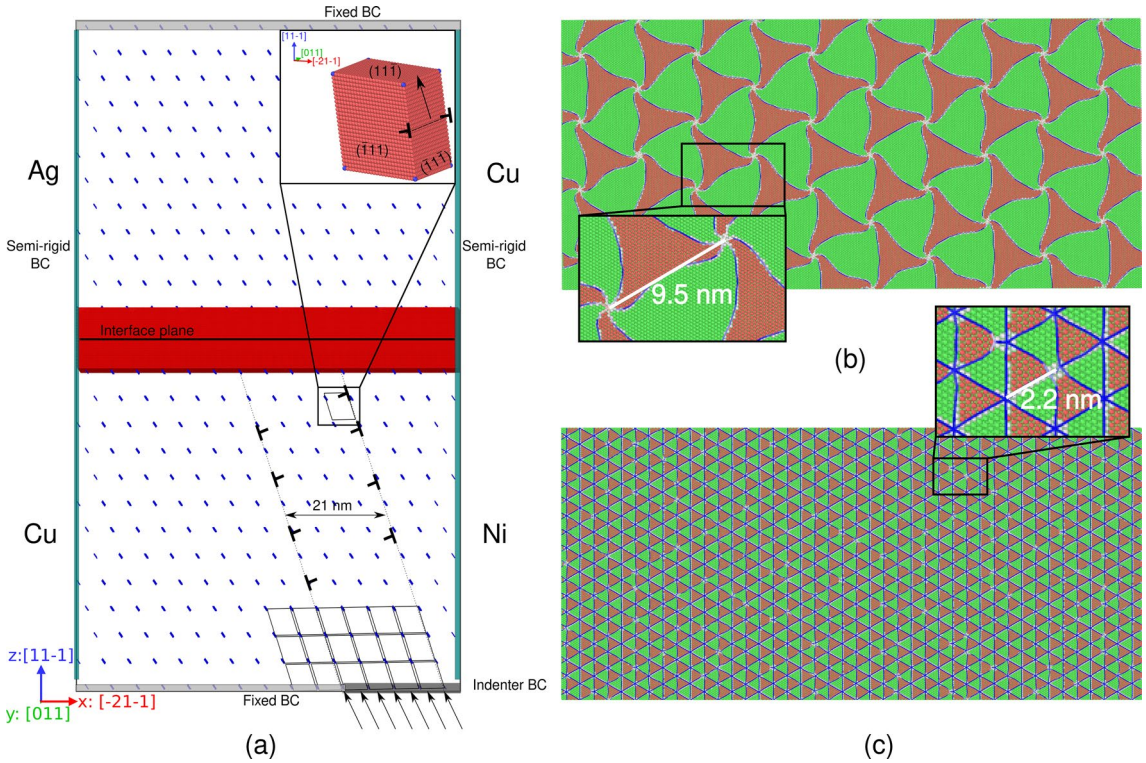

Figure 8: (a) Atom (red) and finite element node (blue) representation of model with overlaid schematics of boundary conditions and CAC finite element shapes. (b) Common neighbor analysis of relaxed Ni/Cu interface and (c) common neighbor analysis of relaxed Cu/Ag interface. Green atoms are FCC, red atoms are HCP, blue atoms are BCC, and gray atoms are others. Insets represent zoomed in sections of interfaces capturing misfit nodes. Misfit node spacings of 9.5 nm and 2.2 nm agree with values from the literature [21].

model as follows. First, atoms within 2 nm of the interface on either side in the test model were mapped to the nearest atom in the reference model. Then, the error metric is computed as the distance between an atom at the interface and its nearest counterpart in the reference model. The model schematic and results of this sensitivity study are shown in Fig. 9. Convergence in the error based on comparison with the most highly refined solution occurs for models having more than approximately 16 atomic layers; accordingly, the models are constructed with 16 atomic layers on each side of the interface. This is equivalent to an atomic layer thickness of 5 nm from the interface to the coarse-grained region. This is larger than the minimum thicknesses of 1.2 nm required for strontium-titanate grain boundaries [48], and larger than those used in some previous CAC simulations of approximately 2.2 nm [35] and 3.5 nm [33, 34] thickness from the interface to the coarse-grained region. This difference likely results from the highly mobile misfit dislocations within the bimetal interfaces that require large displacements to form the spiral misfit pattern that are not present in the previously discussed interfaces. The small amounts of uniformly distributed error at higher numbers of atomic layers results from uniform shifts in interface position across periodic boundaries. This minimum number of atomic layers is also used for the Cu/Ag model, as the minimization of the Cu/Ag interface is accompanied by much smaller changes to the misfit dislocation structure than in the Ni/Cu interface.

As shown in Fig. 8, the orientations for the model are $x = [\bar{2}11]$, $y = [011]$, $z = [11\bar{1}]$. Periodic boundaries are enforced in the x and y directions and care is taken when setting model dimensions in order to ensure that periodicity of the interface structure and the bulk layers is maintained. The model has dimensions of $x \approx 82.35$ nm, $y \approx 38.34$ nm, and $z \approx 69.00$ nm corresponding to a layer thickness of 34.5 nm for the Ni/Cu model. The Cu/Ag model has dimensions of $x \approx 80.15$ nm, $y \approx 37.59$ nm, and $z \approx 74.52$ nm corresponding to a layer thickness of approximately 37.3 nm. To generate dislocations on specific intersecting slip planes, elements and atoms within a rectangular region at the bottom surface are effectively indented along interelement discontinuities generating 60° mixed character dislocations on distinct slip planes that are offset by approximately 21 nm. This is done by prescribing a displacement to the portion of atoms and nodes with x positions between 38 and 59 nm at the bottom surface and keeping all other atoms and nodes at the surface fixed. This simple approach to imposing indentation is satisfactory for the purpose of generating distinct dislocations to study the evolution of interface structure as a result of dislocation stress fields [30]. For both models, indentation is performed on the bulk material which has the

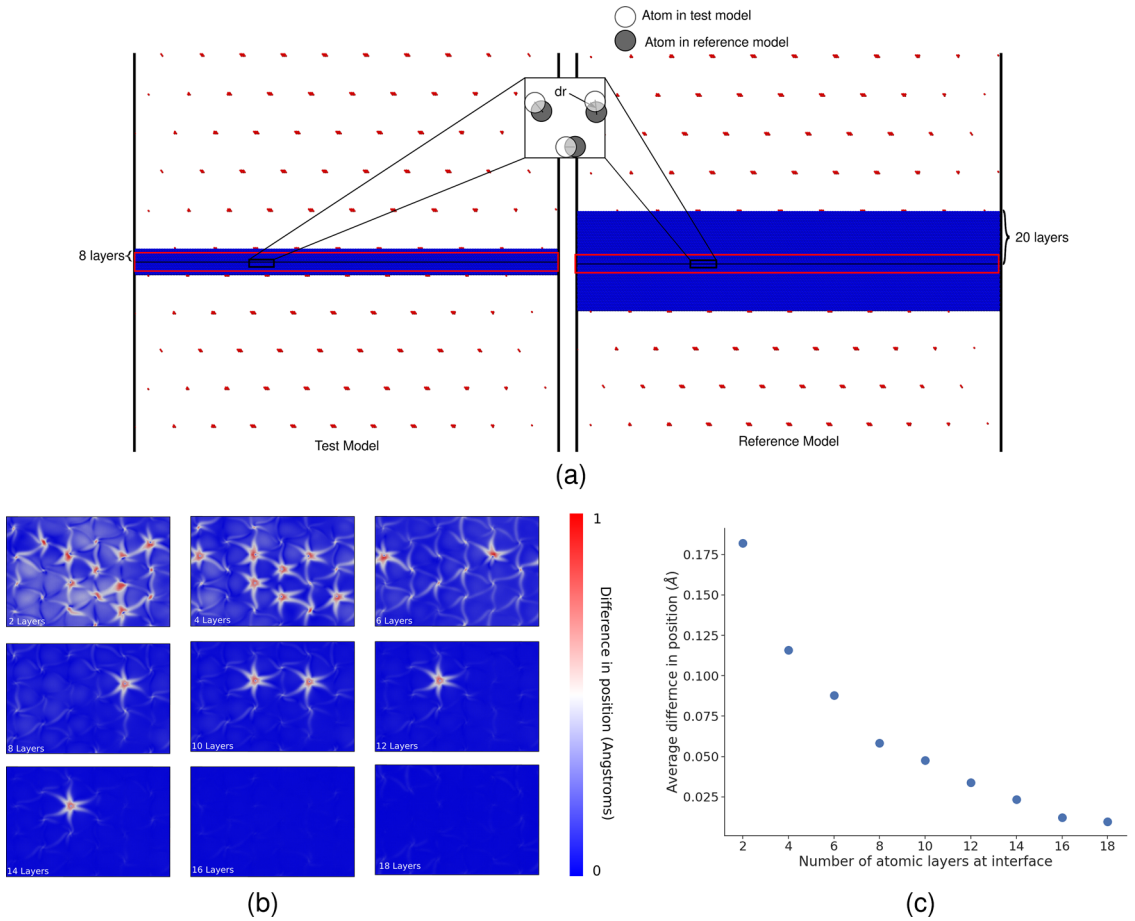

Figure 9: (a) Schematic of mesh sensitivity models showing calculation of "dr" which is the difference in atom position between an atom in the test model and the atom in the reference model. (b) Local error maps of the interface show error in the minimization of the Ni/Cu interface primarily associated with interface nodes which have high degrees of restructuring. (c) The error plot shows that convergence of atomic positions is reached at approximately 16 atomic layers.

smaller lattice constant, i.e. Ni in the Ni/Cu system and Cu in the Cu/Ag system, such that lattice dislocations are under tensile coherency stresses from the interface. This is to compare the lattice dislocation induced misfit dislocation evolution for different misfit dislocation node spacings under similar stress states. Future studies will investigate whether the interaction of dislocation stress fields with the interface coherency stress fields of the originating bulk material, the sign of which depends on whether the bulk material has the larger or smaller lattice constant, causes differing interface misfit dislocation structure evolution that contributes to the direction-dependent slip transmission blocking strength observed in the literature [12, 49].

Dislocations are generated on intersecting $(\bar{1}1\bar{1})$ slip planes. Other more complex methods for simulating indentation exist for predicting hardness from atomistic simulations [50, 51]. The displacement magnitude at every indentation step is 0.3 Å. Three 60° mixed character dislocations are generated per plane with a max indentation step of 6.6 Å. A small degree of asymmetry is noted in the progression of dislocations on both slip planes. Dislocations are found to progress first along the slip plane which impinges on the interface closer to the center of the model. This small asymmetry likely arises from the difference in the proximity of each slip plane to the semi-rigid boundaries, which may impart additional stresses that hinder the motion of the dislocations. After every indentation step, quenched dynamics [52] is run for 10 ps, or 1000 timesteps, and then energy minimization is performed using FIRE. This approach better approximates the sequence of constrained equilibrium states pertaining to quasistatic deformation under the imposed boundary conditions; simple quasistatic energy minimization, in contrast, can fall into local energy minima in complex energy landscapes. During indentation, semi-rigid boundaries are used for atoms at the boundaries of the cell in the x direction and periodic dimensions are used in the y, or lattice dislocation line, direction. To create a rectangular domain, atoms are used to fill the jagged interstices between coarse-grained elements along all dimensions. To ensure that the indenter distance did not have a significant impact on the interface structures observed, two models with indenter distances of 34.5 nm and

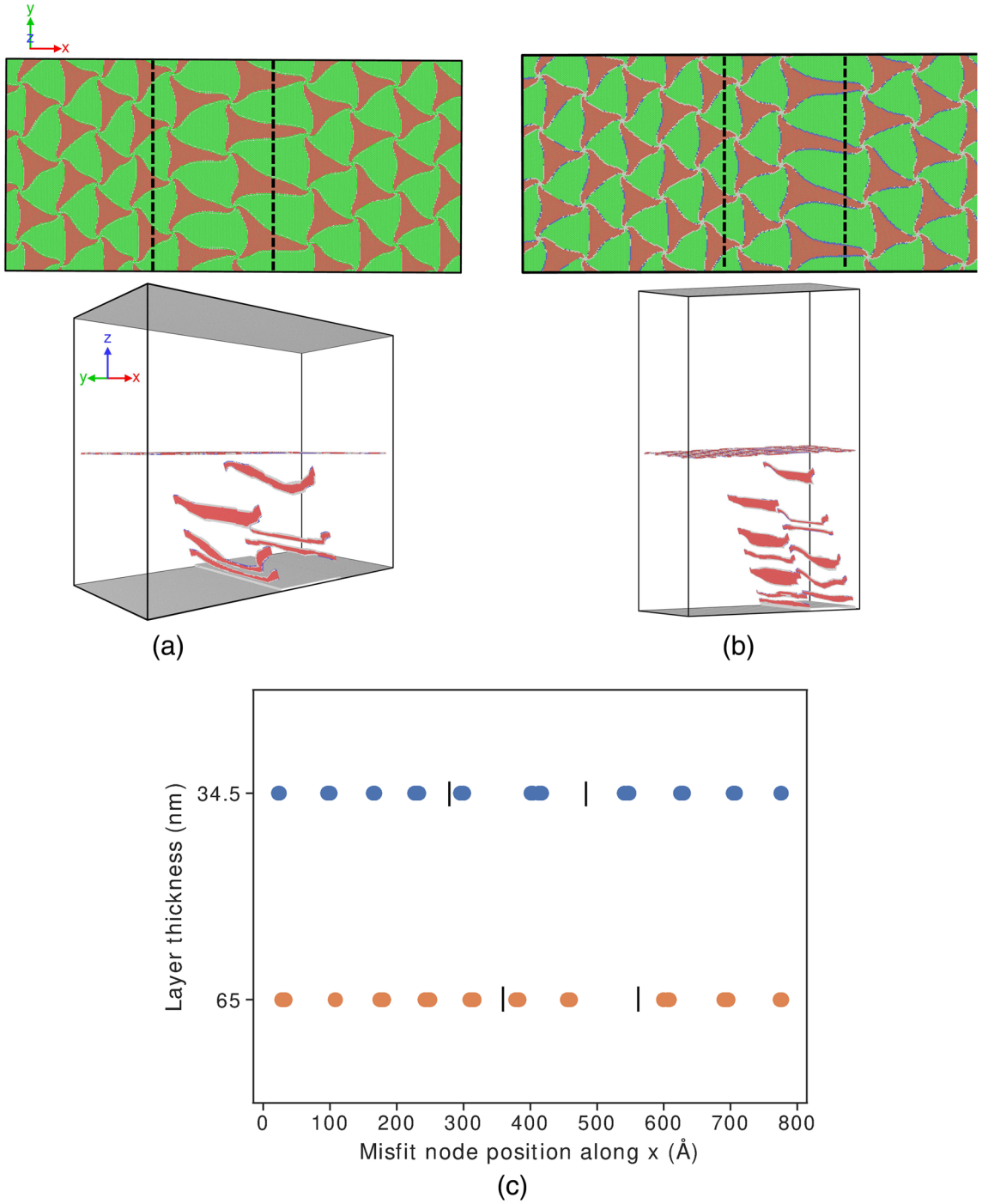

Figure 10: (a) Interface and dislocation structure for the 34.5 nm layer thickness model and (b) 65 nm layer thickness model at the timestep prior to the lattice dislocation entering the interface. (c) Shows the misfit node positions along the x direction with black lines denoting the slip plane impingement sites. Similar structures are seen in both models with increased distance of misfit nodes from the impingement sites in the 65 nm model resulting from the additional shear stress imparted by the long-range fields of the additional dislocations in the pileup.

65 nm from the interface were investigated. Figure 10 shows the interface structure at the indentation step prior to the dislocation entering the interface. The interface misfit structures in both cases are similar. Analysis of the node distribution along the *x* direction also matches in both cases with an increased misfit node distance from the slip plane impingement for the larger model resulting from the increased shear stress induced by additional dislocations in the pileup. The 34.5 nm model was therefore considered to have sufficient separation between indenter and interface for comparing the evolution of misfit patterns for Ni/Cu and Cu/Ag.

The only pertinent constitutive law for both the coarse-grained region and the atomistic region is the interatomic potential. For the Ni/Cu models the interatomic potential developed by Onat and Durukanoğlu is used [53] which accurately captures the stacking fault energies for each individual component and captures the alloy structure energetics accurately. The Williams, Mishin, and Hamilton [54] potential for Cu/Ag is used, which accurately captures the energetics of both bulk and cross-interaction terms. Accordingly, the equilibrium lattice constants are 3.615, 4.09, and 3.52 Å for Cu, Ag, and Ni, respectively. All simulations are run using the PyCAC code [55]. To visualize the models, coarse-grained regions are converted to the equivalent atomistic model and OVITO [56] is used. The Dislocation Extraction Algorithm (DXA) [57] is used for visualizing dislocations. Common neighbor analysis (CNA) [58] is used for the visualization of atomic structures and qualitative comparisons. In so doing, a variety of continuum metrics can be computed based on relative motion of local neighborhood of each atom to promote enhanced understanding of the structural evolution. In particular, the microrotation is an informative metric to quantify in more detail the interface reconstruction [44] and is defined by the vector:

$$\phi_k = -\frac{1}{2}\varepsilon_{ijk}(R_{\text{skew}})_{ij} \tag{1}$$

where ε is the permutation symbol and R_{skew} is the skew symmetric part of the rotation tensor in the polar decomposition of the deformation gradient, i.e.,

$$\mathbf{F} = \mathbf{RU} \tag{2}$$

$$R_{skew} = \frac{1}{2}(R - R^{\mathrm{T}}) \tag{3}$$

Here, **R** is the rotation, **U** is the right stretch tensor, and **F** is the deformation gradient, computed within some finite radius of each atom containing only first nearest neighbors. To calculate the rotation tensor, first the deformation gradient F is calculated from the current and reference atomic configurations. The right stretch tensor U is then computed using:

$$\mathbf{U} = \sqrt{\mathbf{F}^{\mathrm{T}}\mathbf{F}} \tag{4}$$

The rotation tensor can then be computed from **F** and the inverse of **U.** More in-depth descriptions on the calculation of the deformation gradient and microrotation for atomistics can be found in [59, 60].

Acknowledgments

This work is based on research supported by the National Science Foundation under the Grants CMMI-1761553 and CMMI-1761512. All presented simulations were conducted using XSEDE resources under allocation TG-MSS150010.

References

1. X. Wu, P. Jiang, L. Chen, F. Yuan, Y.T. Zhu, Extraordinary strain hardening by gradient structure. Proc. Natl. Acad. Sci. **111**(20), 7197–7201 (2014)
2. X. Wu, M. Yang, F. Yuan, G. Wu, Y. Wei, X. Huang, Y. Zhu, Heterogeneous lamella structure unites ultrafine-grain strength with coarse-grain ductility. Proc. Natl. Acad. Sci. **112**(47), 14501–14505 (2015)
3. J. Moering, X. Ma, G. Chen, P. Miao, G. Li, G. Qian, S. Mathaudhu, Y. Zhu, The role of shear strain on texture and microstructural gradients in low carbon steel processed by surface mechanical attrition treatment. Scripta Mater. **108**, 100–103 (2015)
4. A. Misra, 7—mechanical behavior of metallic nanolaminates, in *Nanostructure control of materials*. ed. by R.H.J. Hannink, A.J. Hill (Woodhead Publishing, Sawston, 2006), pp. 146–176
5. N.A. Mara, I.J. Beyerlein, Interface-dominant multilayers fabricated by severe plastic deformation: stability under extreme conditions. Cur. Opin. Solid State Mater Sci. **19**(5), 265–276 (2015)
6. C.C. Tasan, M. Diehl, D. Yan, M. Bechtold, F. Roters, L. Schemmann, C. Zheng, N. Peranio, D. Ponge, M. Koyama et al., An overview of dual-phase steels: advances in microstructure oriented processing and micromechanically guided design. Annu. Rev. Mater. Res. **45**, 391–431 (2015)
7. A. Sáenz-Trevizo, A.M. Hodge, Nanomaterials by design: a review of nanoscale metallic multilayers. Nanotechnology **31**(29), 292002 (2020)
8. B.M. Clemens, H. Kung, S.A. Barnett, structure and strength of multilayers. MRS Bull. **24**(2), 20–26 (1999)
9. Q. Zhou, J.Y. Xie, F. Wang, P. Huang, K.W. Xu, T.J. Lu, The mechanical behavior of nanoscale metallic multilayers: a survey. Acta Mech. Sin. **31**(3), 319–337 (2015)
10. R.G. Hoagland, R.J. Kurtz, C.H. Henager, Slip resistance of interfaces and the strength of metallic multilayer composites. Scripta Mater. **50**(6), 775–779 (2004)
11. I.N. Mastorakos, H.M. Zbib, D.F. Bahr, Deformation mechanisms and strength in nanoscale multilayer metallic composites with coherent and incoherent interfaces. Appl. Phys. Lett. **94**(17), 173114 (2009)
12. M. Xiang, Y. Liao, K. Wang, G. Lu, J. Chen, Shock-induced plasticity in semi-coherent 111 cu-ni multilayers. Int J. Plast. **103**, 23–38 (2018)
13. S. Shao, J. Wang, I.J. Beyerlein, A. Misra, Glide dislocation nucleation from dislocation nodes at semi-coherent 1 1 1 Cu–Ni interfaces. Acta Mater. **98**, 206–220 (2015)
14. X.Y. Chen, X.F. Kong, A. Misra, D. Legut, B.N. Yao, T.C. Germann, R.F. Zhang, Effect of dynamic evolution of misfit dislocation pattern on dislocation nucleation and shear sliding at semi-coherent bimetal interfaces. Acta Mater. **143**, 107–120 (2018)

15. H. Yang, L. Zhu, R. Zhang, J. Zhou, Z. Sun, Influence of high stacking-fault energy on the dissociation mechanisms of misfit dislocations at semi-coherent interfaces. Int J. Plast. **126**, 102610 (2020)
16. R.F. Zhang, T.C. Germann, X.Y. Liu, J. Wang, I.J. Beyerlein, Layer size effect on the shock compression behavior of fcc–bcc nanolaminates. Acta Mater. **79**, 74–83 (2014)
17. R. Dikken, M. Khajeh Salehani, Edge dislocation impingement on interfaces between dissimilar metals (2017)
18. A. Couret, J. Crestou, S. Farenc, G. Molenat, N. Clement, A. Coujou, D. Caillard, In situ deformation in T.E.M: recent developments. Microsc. Microanal. Microstruct. **4**(2–3), 153–170 (1993)
19. S. Shao, J. Wang, A. Misra, R.G. Hoagland, Spiral patterns of dislocations at nodes in (111) semi-coherent FCC interfaces. Sci. Rep. (2013). https://doi.org/10.1038/srep02448
20. H. Yang, L. Zhu, R. Zhang, J. Zhou, Z. Sun, Shearing dominated by the coupling of the interfacial misfit and atomic bonding at the FCC (111) semi-coherent interfaces. Mate Des. **186**, 108294 (2020)
21. S. Shao, J. Wang, A. Misra, Energy minimization mechanisms of semi-coherent interfaces. J. Appl. Phys. **116**(2), 023508 (2014)
22. E.B. Tadmor, M. Ortiz, R. Phillips, Quasicontinuum analysis of defects in solids. Philos. Mag. A **73**(6), 1529–1563 (1996)
23. E.B. Tadmor, F. Legoll, W.K. Kim, L.M. Dupuy, R.E. Miller, Finite-temperature quasi-continuum. Appl. Mech. Rev. (2013). https://doi.org/10.1115/1.4023013
24. L.E. Shilkrot, R.E. Miller, W.A. Curtin, Coupled atomistic and discrete dislocation plasticity. Phys. Rev. Lett. (2002). https://doi.org/10.1103/PhysRevLett.89.025501
25. G. Anciaux, T. Junge, M. Hodapp, J. Cho, J.-F. Molinari, W.A. Curtin, The coupled atomistic/discrete-dislocation method in 3d part I: Concept and algorithms. J. Mech. Phys. Solids **118**, 152–171 (2018)
26. D.L. McDowell, Multiscale modeling of interfaces, dislocations, and dislocation field plasticity, in *Mesoscale models*. ed. by S. Mesarovic, S. Forest, H. Zbib (Springer, Cham, 2018)
27. M. Dewald, W.A. Curtin, Analysis and minimization of dislocation interactions with atomistic/continuum interfaces. Model. Simul. Mater. Sci. Eng.. **14**(3), 497–514 (2006)
28. T. Shimokawa, T. Kinari, S. Shintaku, Interaction mechanism between edge dislocations and asymmetrical tilt grain boundaries investigated via quasicontinuum simulations. Phys. Rev. B. (2007). https://doi.org/10.1103/PhysRevB.75.144108
29. Y. Chen, S. Shabanov, D.L. McDowell, Concurrent atomistic-continuum modeling of crystalline materials. J. Appl. Phys. **126**(10), 101101 (2019)
30. S. Xu, R. Che, L. Xiong, Y. Chen, D.L. McDowell, A quasistatic implementation of the concurrent atomistic-continuum method for FCC crystals. Int J. Plast. **72**, 91–126 (2015)
31. S. Xu, D.L. McDowell, I.J. Beyerlein, Sequential obstacle interactions with dislocations in a planar array. Acta Mater. **174**, 160–172 (2019)
32. L. Xiong, D.L. McDowell, Y. Chen, Nucleation and growth of dislocation loops in Cu, Al and Si by a concurrent atomistic-continuum method. Scripta Mater. **67**(7–8), 633–636 (2012)
33. S. Xu, L. Xiong, Y. Chen, D.L. McDowell, Sequential slip transfer of mixed-character dislocations across Σ3 coherent twin boundary in FCC metals: a concurrent atomistic continuum study. npj Comput. Mater. **2**(1), 15016 (2016)
34. S. Xu, L. Xiong, Y. Chen, D.L. McDowell, Comparing EAM potentials to model slip transfer of sequential mixed character dislocations across two symmetric tilt grain boundaries in Ni. JOM **69**(5), 814–821 (2017)
35. S. Xu, Y. Li, and Y. Chen: Si/Ge (111) semicoherent interfaces: Responses to an in-plane shear and interactions with lattice dislocations. *Physica Status Solidi (b)*. 257, 2000274 (2020).
36. Y. Li, Z. Fan, W. Li, D.L. McDowell, Y. Chen, A multiscale study of misfit dislocations in PbTe/PbSe(001) heteroepitaxy. J. Mater. Res. **34**(13), 2306–2314 (2019)
37. H. Chen, S. Xu, W. Li, R. Ji, T. Phan, L. Xiong, A spatial decomposition parallel algorithm for a concurrent atomistic-continuum simulator and its preliminary applications. Comput. Mater. Sci. **144**, 1–10 (2018)
38. W.-R. Jian, M. Zhang, S. Xu, I.J. Beyerlein, Atomistic simulations of dynamics of an edge dislocation and its interaction with a void in copper: A comparative study. Modell. Simul. Mater. Sci. Eng. **28**(4), 045004 (2020)
39. G.H. Vineyard, Frequency factors and isotope effects in solid state rate processes. J. Phys. Chem. Solids **3**(1–2), 121–127 (1957)
40. A.F. Voter, J.D. Doll, Transition state theory description of surface self-diffusion: comparison with classical trajectory results. J. Chem. Phys. **80**(11), 5832–5838 (1984)
41. S. Ryu, K. Kang, W. Cai, Predicting the dislocation nucleation rate as a function of temperature and stress. J. Mater. Res. **26**(18), 2335–2354 (2011)
42. G. Henkelman, B.P. Uberuaga, H. Jónsson, A climbing image nudged elastic band method for finding saddle points and minimum energy paths. J. Chem. Phys. **113**(22), 9901–9904 (2000)
43. X. Zhang, B. Zhang, Y. Mu, S. Shao, C.D. Wick, B.R. Ramachandran, W.J. Meng, Mechanical failure of metal/ceramic interfacial regions under shear loading. Acta Mater. **138**, 224–236 (2017)
44. G.J. Tucker, J.A. Zimmerman, D.L. McDowell, Continuum metrics for deformation and microrotation from atomistic simulations: application to grain boundaries. Int. J. Eng. Sci. **49**(12), 1424–1434 (2011)
45. I. Wang, Atomistic simulations of dislocation pileup: grain boundaries interaction. JOM **67**(7), 1515–1525 (2015)

46. M. Dodaran, J. Wang, Y. Chen, W.J. Meng, S. Shao, Energetic, structural and mechanical properties of terraced interfaces. Acta Mater. **171**, 92–107 (2019)
47. E. Bitzek, P. Koskinen, F. Gähler, M. Moseler, P. Gumbsch, Structural relaxation made simple. Phys. Rev. Lett. **97**(17), 170201 (2006)
48. S. Yang, Y. Chen, Concurrent atomistic and continuum simulation of bi-crystal strontium titanate with tilt grain boundary. Proc. R. Soc. A Math. Phys. Eng. Sci. **471**(2175), 20140758 (2015)
49. X. Tian, J. Cui, M. Yang, K. Ma, M. Xiang, Molecular dynamics simulations on shock response and spalling behaviors of semi-coherent 111 Cu-Al multilayers. Int. J. Mech. Sci. **172**, 105414 (2020)
50. C. Ruestes, I. Alhafez, H. Urbassek, C.J. Ruestes, I.A. Alhafez, H.M. Urbassek, Atomistic studies of nanoindentation—a review of recent advances. Curr. Comput.-Aided Drug Des. **7**(10), 293 (2017)
51. S.Z. Chavoshi, S. Xu, Nanoindentation/scratching at finite temperatures: Insights from atomistic-based modeling. Prog. Mater Sci. **100**, 1–20 (2019)
52. E. Tadmor, *Modeling Materials: Continuum, Atomistic, and Multiscale Techniques* (Cambridge University Press, Cambridge, New York, 2011).
53. B. Onat, S. Durukanoglu, An optimized interatomic potential for Cu-Ni alloys with the embedded-atom method. J. Phys. Condens. Matter (2014). https://doi.org/10.1088/0953-8984/26/3/035404
54. P.L. Williams, Y. Mishin, J.C. Hamilton, An embedded-atom potential for the Cu–Ag system. Modell. Simul. Mater. Sci. Eng. **14**(5), 817–833 (2006)
55. S. Xu, T.G. Payne, H. Chen, Y. Liu, L. Xiong, Y. Chen, D.L. McDowell, PyCAC: The concurrent atomistic-continuum simulation environment. J. Mater. Res. **33**(7), 857 (2018)
56. A. Stukowski, Visualization and analysis of atomistic simulation data with OVITO–the open visualization tool. Modell. Simul. Mater. Sci. Eng. **18**(1), 015012 (2009)
57. A. Stukowski, K. Albe, Dislocation detection algorithm for atomistic simulations. Modell. Simul. Mater. Sci. Eng. **18**(2), 025016 (2010)
58. D. Faken, H. Jónsson, Systematic analysis of local atomic structure combined with 3D computer graphics. Comput. Mater. Sci. **2**(2), 279–286 (1994)
59. I.A. Zimmerman, D.J. Bammann, H. Gao, Deformation gradients for continuum mechanical analysis of atomistic simulations. Int. J. Solids Struct. **46**(2), 238–253 (2009)
60. G.J. Tucker, J.A. Zimmerman, D.L. McDowell, Shear deformation kinematics of bicrystalline grain boundaries in atomistic simulations. Modell. Simul. Mater. Sci. Eng. **18**(1), 015002 (2009)